HEX-TASEP: dynamics of pinned domains for TASEP transport on a periodic lattice of hexagonal topology

2008 J. Phys.: Condens. Matter 20 295213

(http://iopscience.iop.org/0953-8984/20/29/295213)

IOP PUBLISHING JOURNAL OF PHYSICS: CONDENSED MATTER

J. Phys.: Condens. Matter **20** (2008) 295213 (8pp) doi:10.1088/0953-8984/20/29/295213

HEX-TASEP: dynamics of pinned domains for TASEP transport on a periodic lattice of hexagonal topology

Ben Embley[1,2], Andrea Parmeggiani[3] and Norbert Kern[2]

[1] School of Chemical Engineering and Analytical Science, The University of Manchester, PO Box 88, Sackville Street, Manchester M60 1QD, UK
[2] Laboratoire des Colloïdes, Verres et Nanomatériaux, CNRS-UMR5587, CC 069, Université Montpellier II, Place Eugène Bataillon, 34095 Montpellier Cedex 5, France
[3] Laboratoire de Dynamique des Interactions Membranaires Normales et Pathologiques, CNRS-UMR 5235, CC107, Université Montpellier II, Place Eugène Bataillon, 34095 Montpellier Cedex 5, France

E-mail: norbert.kern@lcvn.univ-montp2.fr

Received 30 November 2007
Published 1 July 2008
Online at stacks.iop.org/JPhysCM/20/295213

Abstract
We investigate a totally asymmetric simple exclusion process (TASEP) on a periodic hexagonal lattice with a single unit cell. We first explain the resulting stationary density profiles and the resulting fundamental current–density relation in terms of mean-field arguments. For intermediate overall densities, transport through one of the segments saturates in a maximum current phase, whereas the others develop domain walls of fixed height but fluctuating position. Via kinetic Monte Carlo simulations we focus on and fully characterize their non-equilibrium and stochastic phenomenology. We invoke a picture of anticorrelated domain wall dynamics, which we visualize as a diffusing obstruction of constant size ('jam'). The role of the boundary conditions is discussed by comparing the periodic lattice carrying a fixed number of particles to a system coupled to reservoirs at open boundaries which is periodic only on average. We highlight the differences in their dynamics based on a novel visualization of domain wall motion at an intermediate 'mesoscopic' timescale.

(Some figures in this article are in colour only in the electronic version)

1. Introduction

A variety of laboratory systems has revealed interesting physics which may be described in terms of transport on 1D or quasi-1D structures: the motion of colloidal particles in narrow channels [1] or in beams of an optical trap [2], the transport and force production of molecular motors on bio-filaments [3–5] and the diffusion of chemical species on zeolites [6] may be cited as examples. Their phenomenology can be rich and subtle, but many of the main features of the associated transport phenomena may be understood in terms of a totally asymmetric simple exclusion process (TASEP) on a lattice [7–11], which has particularly simple rules: at regular intervals randomly selected particles advance one site in a fixed direction, subject only to an excluded volume condition forbidding multiple occupancy. TASEP not only constitutes a perfect toy model for many fundamental questions [12], but often also provides valuable guidance to identifying the main features of a particular transport mechanism (indeed, TASEP was initially formulated to schematize ribosome traffic in gene expression [7]).

In this paper we address the point that, in many situations, transport may in fact take place on a *network* of such quasi-1D segments, linking them at particular points which we will call 'junctions'. Without attempting to model the following in any detail at this stage, we cite examples from various domains: active transport of molecular motors on a structure of crosslinked filaments [13]; advection of particles in the fluid phase of a foam, in particular in foam drainage when the particle size is comparable to that of the channels

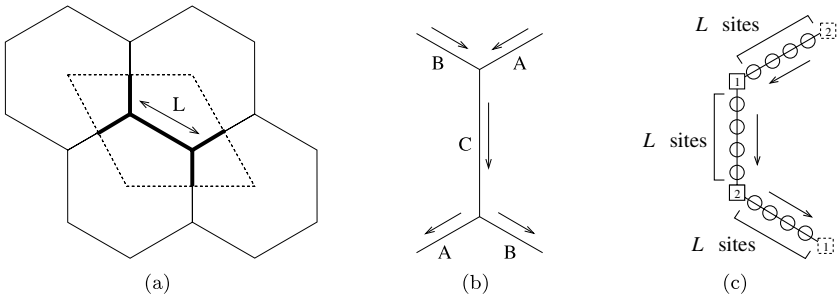

Figure 1. Illustration of the network used. (a) A hexagonal lattice is decomposed into unit cells, to which periodic boundary conditions are applied. (b) The network is therefore constructed from three segments of L lattice sites each, with two additional sites for the junctions. We label the 'central' branch by C, and the 'split' branches by A and B, respectively. (c) The segments, junctions and boundary conditions as implemented. Dotted boxes are the periodically equivalent copies of the corresponding full boxes.

(a case complementary to [14]); traffic of vehicles on road networks [15].

Attempts to characterize TASEP transport on isolated elements of a network have been made in the past; in particular, studies of the effect of a single junction [16] and of a double section [17] have been performed, both using open boundary conditions, and have also been considered for vehicular traffic [18]. Here, we present a systematic study of TASEP transport on a *periodic* hexagonal structure, which we denote HEX-TASEP, and show that the role of fluctuations in the transport process may be pinpointed particularly clearly. We expose and analyse the resulting dynamics within this system, and show that it may be visualized as the diffusive motion of a high-density region of particles (a 'jam') pinned to the junctions. We then address the question of boundary conditions, by comparing the transport on this periodic structure to a related open structure with particle reservoirs. We characterize fluctuations and make a link with the domain wall picture [19], most rigorously exploited on linear sections [20].

2. The model: TASEP on a periodic lattice of hexagonal topology (HEX-TASEP)

We consider TASEP dynamics on a *periodic* hexagonal lattice, as illustrated in figure 1(a). To this end, we simulate one unit cell composed of three branches, comprising one 'central' branch C and two 'split' branches A and B, each consisting of $L = 100$ lattice sites[4]. These branches are connected via an additional site at each junction in the manner illustrated in figures 1(b) and (c), thereby enforcing periodic boundary conditions. This is arguably the simplest periodic structure involving branches, the dynamics of which we set out to explore in view of guidance for the study of more complex networks. Particle moves are attempted according to a random sequential update scheme: in each cycle, we select $3L+2$ sites, which sets our time unit; particle displacements are always attempted according to the directions indicated, and fail if the new site is already occupied. At the network junction, where branch C splits into branches A and B, we select either with equal probability.

[4] Although we do not present a systematic discussion of finite size effects here, we note that none of the phenomena described are artefacts.

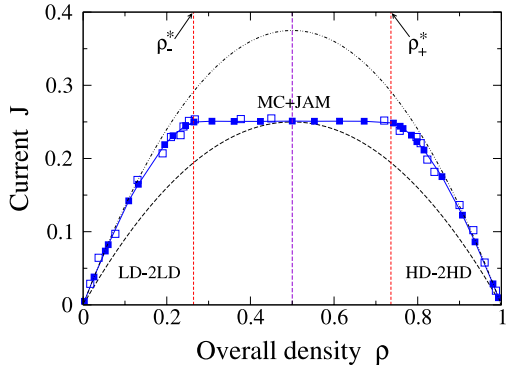

Figure 2. Fundamental diagram for the overall transport characteristics for HEX-TASEP on a periodic hexagonal lattice (full squares), showing the (average) current J as a function of the overall particle density ρ. For comparison, the dashed line (below) represents simple TASEP characteristics, as explained in detail in the text, whereas the dot–dashed line (above) represents TASEP with a projected density $\rho_{\rm proj} \approx 3\rho/2$. The labels correspond to a mean-field classification (cf figure 3). Open squares correspond to the open system to be discussed in section 7, and include non-periodic configurations: on the plateau, $\rho = 0.50$ is the only point corresponding to a periodic (average) density profile.

Initial configurations are constructed from a random distribution of the desired number of particles over all branches, which we then run until a stationary state is achieved, i.e. until the time-averaged density profile $\bar{\rho}(x)$ no longer changes in time (typically 10^6 cycles).

3. Transport characteristics

The overall particle density $\rho = N/(3L+2)$ is the only control parameter in this model, and we therefore start our analysis with the overall transport capacity of the system, characterized by the average current $J(\rho)$ (cf figure 2), defined as the number of particles passing branch C per unit time.

The observed transport is always *superior* to that in standard TASEP without split branches (dashed parabola), as must be the case. The initial slope in $J(\rho)$ at low densities follows what one would predict from an *effective* TASEP, arguing that the relevant particle density is a *projected* density $\rho_{\rm proj} = \frac{N}{2L+2} \approx \frac{3}{2}\rho$, since the actual distance a particle has to

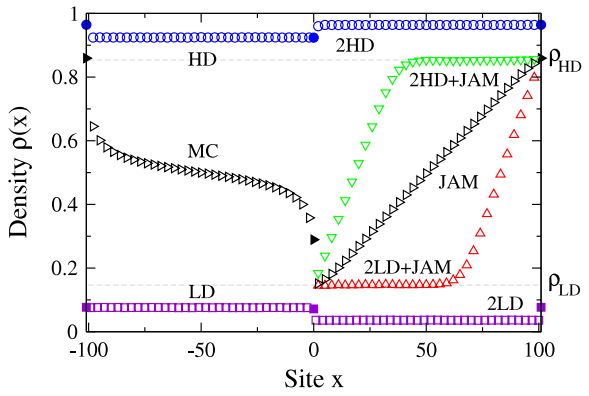

Figure 3. Density profiles for various overall densities ρ, averaged over long times (10^6 cycles). The sites $x < 0$ are the middle branch C, whereas sites $x > 0$ correspond to the split branch A; full symbols represent the junction sites $(0, \pm 101)$. Results for B (not shown) are indistinguishable. The densities shown are selected to illustrate the different density regions introduced in figure 2: $\rho = 0.05$ (squares) corresponds to low-density phases in the central as well as in both split branches (labels LD and 2LD); $\rho = 0.95$ (circles) leads to the high-density equivalent (labels HD and 2HD). For all densities within the zone of saturated current ($0.264 \lesssim \rho \lesssim 0.736$), the maximum current profiles (MC) in the central branch are indistinguishable. In the split branches, close-to-linear zones (JAM) arise in the density profiles in addition to HD or LD zones (examples shown: $\rho = 0.35$ and 0.65, upwards and downwards pointing triangles); for $\rho = 0.5$ the entire split profile is almost linear.

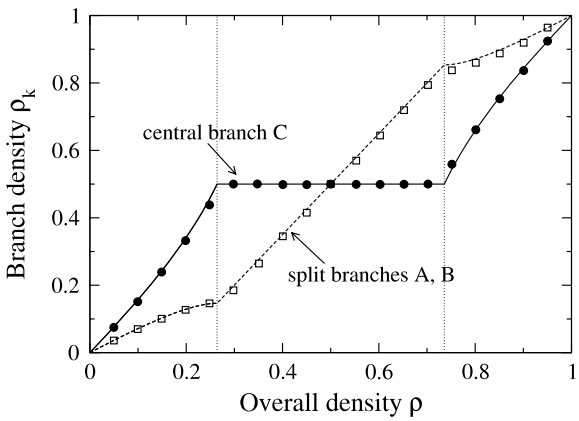

Figure 4. Particle densities in individual branches of HEX-TASEP with periodic boundary conditions, as a function of the *overall* particle density. Lines are mean-field results; symbols indicate simulation data, averaged over 10^6 cycles. As the overall density is increased beyond the critical density ρ_-^*, the central branch develops an MC phase into which, on average, no further particles can be accepted.

travel in order to cross a unit cell is $2L$ (not $3L$). This amounts to saying that, for low densities, particle collisions are rare, and therefore the presence of an extra segment in the split section of the network has a negligible effect. More interestingly, however, at a density $\rho \gtrsim 0.26$ the current saturates at a value of $J_{\max} = 0.25$, which corresponds to the mean-field prediction [8] for a maximum current phase. This maximum value is achieved on a large plateau of intermediate densities ($0.26 \lesssim \rho \lesssim 0.74$). The transport characteristic curve $J(\rho)$ furthermore obeys the particle–hole symmetry; focusing on densities $\rho \leqslant 1/2$ is therefore, in principle, sufficient.

We shall first pursue a more detailed analysis of this periodic hexagonal model, before returning to the fact that an identical $J(\rho)$ curve has also been obtained in a related but different system [17], thereby posing the question of the role of boundary conditions.

4. Mean-field analysis: low-/high-density regions

Beyond the global transport characteristics, it is instructive to examine particle density profiles, i.e. the time-averaged particle densities $\rho(x)$ on site x. Figure 3 shows such profiles, averaged over an entire simulation (10^6 cycles), for various values of the overall density. We can rationalize them using mean-field arguments based on a standard (line topology) TASEP model, which is known to display low-density (LD), high-density (HD) or maximum current (MC) phases [8, 9]. Due to particle conservation, the currents in the individual branches must add up as

$$J \equiv J_{\rm C} = J_{\rm A} + J_{\rm B}. \qquad (1)$$

Furthermore, in a mean-field stationary state, the split branches must behave symmetrically (on average), and therefore $\rho_{\rm A} = \rho_{\rm B} \equiv \rho_{\rm AB}$ and $J_{\rm A} = J_{\rm B} \equiv J_{\rm AB}$. For low overall particle densities ρ, all branches must be in an LD phase. Assuming now the mean-field expression, $J_k = \rho_k (1 - \rho_k)$, to hold in any of the branches $k = $ A, B, C, we obtain

$$\rho_{\rm AB} (1 - \rho_{\rm AB}) = \tfrac{1}{2} \rho_{\rm C} (1 - \rho_{\rm C}). \qquad (2)$$

We can now use the overall conservation of particles $\rho \approx \frac{1}{3}(\rho_{\rm C} + 2\rho_{\rm AB})$ to solve for the densities $\rho_{\rm C}$ and $\rho_{\rm AB}$, respectively. The algebra being straightforward, we do not quote the full expression here, but indicate that figure 4 highlights the excellent agreement with simulation data. Solving analytically for the overall density ρ at which the density in the central branch reaches $\rho_{\rm C} = \rho_{\rm MC} = 1/2$, the mean-field value for a MC phase, yields an overall density of $\rho_-^* = \frac{1}{2} - \frac{\sqrt{2}}{6} \approx 0.264$, which corresponds very well to the onset of the plateau in figure 2. An equivalent analysis holds for high particle densities, involving coexistence of three HD branches, defining $\rho_+^* = 1 - \rho_-^* \approx 0.736$ for the upper limit of the plateau.

5. Mean-field analysis: plateau of optimum transport

Once the transport plateau (cf figure 2) is reached, the current $J_{\rm C}$ is truncated at a value of $1/4$, which is a telltale sign for a maximum current phase. Indeed, simulations reveal the characteristic density profiles for a MC phase in the central branch C (see figure 3 for a snapshot). We may attempt a mean-field interpretation by recalling first that, on average, a MC phase corresponds not only to a specific current ($J_{\rm MC} = 0.25$), but also to a specific density ($\rho_{\rm MC} = 0.5$). In a mean-field spirit, either of the split branches must carry half the total current, $J_{\rm A} = J_{\rm B} = 1/8$, and imposing the mean-field

expression $J = \rho\,(1-\rho)$ therefore yields low and high average densities in the split sections[5]

$$\rho_{\mathrm{LD,HD}} = \frac{1}{2} \pm \frac{\sqrt{2}}{4}. \tag{3}$$

The profiles obtained by simulation are shown in figure 3, confirming that these densities indeed characterize the split phases, albeit not entirely. Consider e.g. the average profile '2LD + JAM' ($\rho = 0.35$). The part of the split sections adjacent to the inlet (site 1) carries an average particle density which is indistinguishable from the mean-field value $\rho_{\mathrm{LD}} \approx 0.146$. Towards the outlet, however, an almost linear profile arises, which we will now rationalize.

Firstly, once the total particle number is sufficient to establish the MC phase in the central branch, the latter cannot accept any further particles. This is obvious on average (since $\rho_{\mathrm{MC}} = 0.5$, independent of the overall density), but also closely followed instantaneously (90% of all instantaneous configurations correspond to densities of $\rho_{\mathrm{C}} = 0.5 \pm 0.05$, averaged over branch C; data not shown). Therefore, upon increasing the overall density, the extra particles must be stored in the split branches (A, B), where it is natural for them to pile up at the outlet, since the junction joining the two branches constitutes a transport-limiting defect.

Secondly, however, the densities in the split branches are also fixed, on average, to ρ_{LD} or ρ_{HD}. The only way to accommodate extra particles is therefore by coexisting phases of densities ρ_{LD} and ρ_{HD} in the split branches, in a proportion allowing us to match the fixed total number of particles in the system. The central part of figure 4 confirms that this simplistic reasoning is indeed appropriate. Note furthermore that the overall length of the 'HD' zone may be estimated from these arguments as $l_{\mathrm{JAM}} = 6L(\rho - \frac{\sqrt{2}}{6})/(3-\sqrt{2})$, which is indeed well respected.

On the other hand, this implies the existence of *domain walls* [9] in the split branches. This is indeed apparent from the *short-time* local sojourn probability shown in figure 5: each split section carries a domain wall separating a low-density phase (at the inlet) and a high-density phase (at the outlet). The respective densities are almost indistinguishable from the mean-field values $\rho_{\mathrm{LD,HD}}$ (cf equation (3)). We will now characterize the dynamics of these domain walls and show that, in contrast to a previous study with open boundary conditions [17], this allows us to rationalize the above average density profiles entirely.

6. Beyond mean field: phenomenology of correlated domain wall dynamics on the transport plateau

From now on, we focus on the region revealing the most interesting dynamics, $\rho^*_- < \rho < \rho^*_+$, such that the central branch carries a MC phase and domain walls (DWs) arise in the split sections. We base our description on the following observations.

[5] These values have also been stated [16, 17] for the open system to be discussed in section 7.

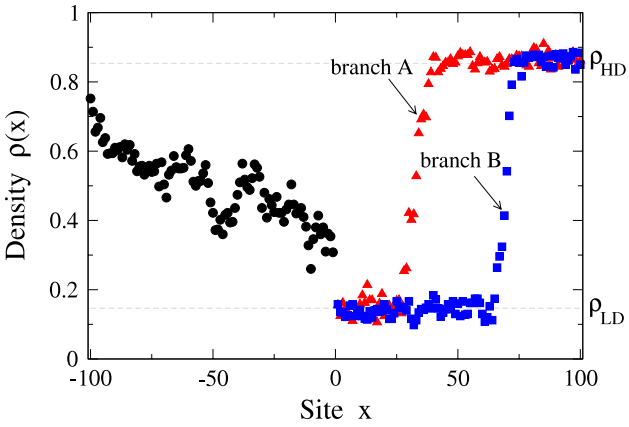

Figure 5. A 'mesoscopic' snapshot of an averaged profile, based on a short-time average (100 cycles), shows that the high-density zones at the outlet instantaneously extend into both split branches. It is a random walk of this 'jam', caused by microscopic fluctuations in the number of particles entering/leaving the split branches A and B, which accounts for these linear profiles (JAM) in the long-time-averaged density profiles in figure 3. A microscopic point of view is detailed in appendix A.

(i) At any instant in time, each split branch carries a low-density zone at its inlet and a high-density zone at its outlet, the two being separated by a domain wall; we may therefore think of a *'jam'* region *pinned* to the outlet junction, extending into both split branches, delimited by a domain wall in each split branch.

(ii) The total number of particles is fixed by the overall density, and the number of extra particles to be accommodated in the split branches has been seen to be approximately constant; the 'jam' may therefore be taken to be of roughly *constant size*, set only by the overall density.

(iii) The stochastic processes at the junctions introduce fluctuations in how the extra particles, and hence the high-density zones, are distributed between the branches; the 'jam' therefore *diffuses* due to these fluctuations.

We rationalize this picture recalling first that the MC phase has a fixed particle density and therefore cannot accommodate any additional particles, necessarily leading to high-density zones in the split branches which are swept to the bottleneck (the junction point). A microscopic representation of the resulting jam's motion may now be motivated by considering a time interval during which, on average, one particle is transported through the maximum current branch (i.e. $\tilde{T} = 1/J_{\mathrm{MC}} = 4$ cycles). This particle must enter one of the split branches, and we may assume it has equal probabilities for choosing either, given that both branches are in an LD phase at the inlet. Similarly, one particle must leave the split section through the outlet, and again we may assume it to originate from either branch with equal probability, given that the outlet zone is HD in both branches. A given branch therefore receives zero or one particles (with probabilities 1/2 each), while losing zero or one particles (with the same probabilities). Since any change in the number of particles in one branch must occur at the expense of that in the other branch, the net effect is therefore that the jam has shifted by the equivalent of 0 or ± 1

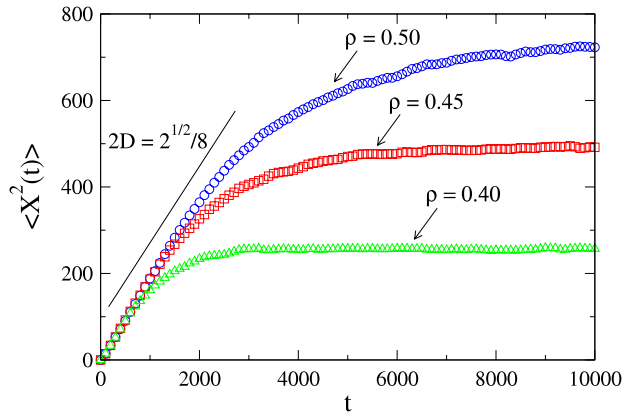

Figure 6. Mean-square displacement for the jam, characterized by the position of its centre X, measured from the junction point, as a function of time. All simulations were started with the jam centre at the outlet. The slope shown is the theoretical prediction (see text). The saturation for long times is due to the finite excursions of the jam, which remains pinned to the downstream junction.

particles. From this process we can deduce a diffusion constant for the jam centre of $D_{\mathrm{JAM}} = \sqrt{2}/16$ in dimensionless units (see appendix A). This is indeed corroborated by numerical data (figure 6) showing the ensemble-averaged mean-square displacement of the centre of the jam.

7. Comparison to an effective system with open boundary conditions

We now address the role of boundary conditions. To do so, we construct a second system, obtained from the hexagonal periodic lattice used above by breaking the periodicity at the middle of the central section and connecting the resulting half-segments to reservoirs (see figure 7). We therefore have a section of length $L/2$ into which particle insertions are attempted with probability α, followed by two split sections of length L, followed by another section of length $L/2$, at the end of which we absorb particles with probability β. This system is very similar[6] to the one studied by Brankov *et al* [17]. To make contact with our system, we may impose $\alpha = 1 - \beta$ [9], which ensures the overall density profile is spatially periodic *on average*.

The open boundaries in this system obviously lead to fluctuations in the number of particles, and the image of a 'jam' undergoing simple diffusive motion must fail. Although the current $J(\rho)$ obtained for a given density ρ is found to be identical to that of a closed system (see figure 2), the underlying fluctuations and the resulting dynamics by which this average transport is achieved are entirely different.

To describe and compare the dynamic behaviour, we introduce a simple method to characterize the system at an intermediate timescale. To this end, we sample density profiles in the split branches A, B, which we average over $\tau = 100$ cycles. At this scale, much larger than the individual cycle but much smaller than the time required for a domain wall to diffuse over the length of an entire branch, we can localize the domain walls in both branches. This 'mesoscopic' approach, further details of which can be found in appendix B, allows us to reliably detect the domain wall positions as well as to

[6] However, each of our single sections has length $L/2$, rather than L, and we do *not* couple moves between both split sections, but treat all particles as independent.

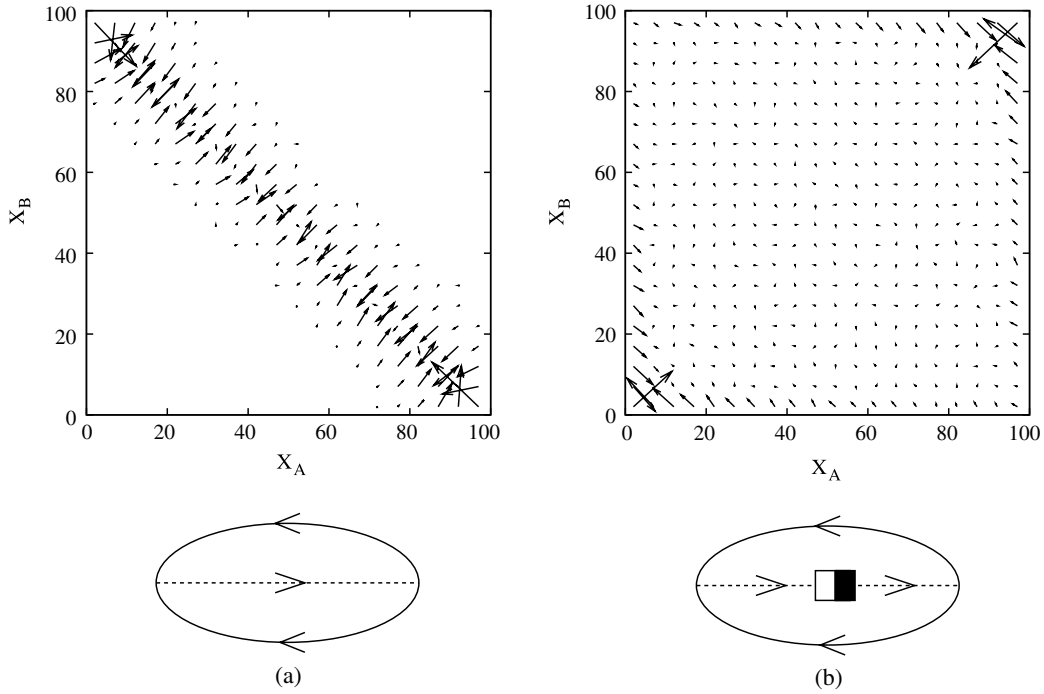

Figure 7. Vector fields characterizing domain wall dynamics at $\rho = 0.5$: arrows indicate the displacement of the domain walls within the next 100 cycles (cf text), as averaged over 10^8 and 3×10^8 cycles, respectively. Results have been coarse-grained over 5×5 positions to improve statistics and rescaled for readability. (a) Periodic hexagonal lattice and (b) branches with two junctions and open boundary conditions ($\alpha = \beta = 1/2$). $X_{\mathrm{A,B}}$ label positions of the domain walls within the split branches (zero corresponds to the inlet).

trace their evolution with time. The dynamics of the system are therefore characterized by the sequence of the domain wall positions $X_A(t)$ and $X_B(t)$ in both split branches.

We then visualize the system's dynamics by representing the *phase space* $\{X_A, X_B\}$. Every time a state point is visited, we detect the subsequent *displacement* with respect to the next domain wall positions; by sampling time averages of these displacements, we build up a vector field representing the time-averaged movement of domain walls. The result for the periodic hexagonal system is shown in figure 7(a), which reflects the features described above: the overall particle number being fixed, the domain wall positions are anticorrelated and restricted roughly to the antidiagonal; deviations are small and redressed by the dynamics; domain wall positions implying large variations in the particle number are essentially forbidden. The longest arrows arise at the corner zones, corresponding to the maximum excursion of the jam region, and are directed along the antidiagonals: once the HD jam has completely swept into one branch, it cannot migrate further (since entering the MC phase, which cannot accept particles, is forbidden); therefore, the HD jam must necessarily return into the branch it has momentarily vacated: the jam undergoes 'reflection' at maximum excursion.

A comparison to the system with open boundary conditions may now be made for $\alpha = \beta = 0.5$, which ensures periodic *averaged* density profiles at a constant *average* overall density of $\rho = 0.5$. The corresponding displacement diagram (figure 7(b)) highlights the complete change in dynamics. Particle number fluctuations due to the reservoirs render all state points accessible, and the domain walls no longer evolve in an anticorrelated manner. Rather, they execute individual random walks (arrows at state points in the central region average out to very small displacements with no particular orientation), except at the edges of the diagram, where 'reflection' is due to the same mechanism.

8. Discussion

In this paper we have introduced topological aspects to the TASEP model, using a hexagonal network structure to illustrate the effects on transport of branching and junctions in a network of periodic topology. We have studied the simplest possible periodic system, a one-cell hexagonal lattice, the understanding of which is crucial before addressing more complex networks. A rich phenomenology arises, involving different regimes according to the overall density, with transitions at critical values which are well predicted by mean-field arguments. In particular, at intermediate densities the fundamental diagram $J(\rho)$ saturates as a dynamic high-density 'jam' forms, pinned to the junction where two branches join. The observed time-averaged density profiles may be interpreted in terms of a random walk of this 'jam' due to microscopic fluctuations. Introducing a 'mesoscopic' characterization of domain wall dynamics, based on the short-time-averaged position of domain walls, the jam is associated with anticorrelated domain wall displacements, and is seen to be reflected at its maximum excursion.

Boundary conditions play an important role, as is illustrated by opposing what might be considered generalizations of the canonical and grand-canonical ensembles for 1D transport: a closed system (periodic, with a fixed number of particles) and an open system (periodic only *on average*, with a given *average* number of particles). Both lead to undistinguishable average transport properties $J(\rho)$, but remarkably these are sustained by entirely different dynamics. This illustrates an important aspect for modelling of transport on networks: whereas an approach in terms of effective rates may be expected to capture the average transport $J(\rho)$, no information may be obtained on the underlying dynamics or even on the resulting average density profiles in the system.

The simple model of HEX-TASEP on a single unit cell therefore constitutes a non-trivial starting point for understanding the role of topology and boundary conditions within driven transport on branched networks. In particular, its relative simplicity makes it a good candidate for a quantitative analysis of the correlations between domain wall motion and their fluctuations, as well as the nature of the transitions between the various dynamical regimes. Generalizations to more complex topologies are clearly to be envisaged. As a lead to follow, we mention a fourfold unit cell, retaining a fully periodic hexagonal structure but relaxing the periodicity on instantaneous particle configurations. Preliminary simulations indicate that the phenomenology is yet more intriguing, but that insight gained in this paper is indeed useful: the four-cell network retains aspects of both the open and the closed single-cell system. We expect progressive generalizations addressing disorder to provide further valuable guidance for the analysis of transport phenomena on disordered networks.

Acknowledgments

BE was supported by an EC Marie Curie Fellowship (MEST-CT-2004-503750). We thank Paul Grassia for encouraging this collaboration and acknowledge Walter Kob and Sébastien Léonard for useful discussions, as well as Walter Kob, Paolo Pierobon and Paul Grassia for a critical reading of a preliminary manuscript.

Appendix A. Jam diffusion coefficient on the transport plateau

In the main text we have related the effective diffusion of the 'jam' to microscopic fluctuations at the inlet and the outlet of the double section (see section 6). Here we provide a detailed derivation of the associated diffusion constant, which is also represented in figure 6. In contrast to the main text, where dimensionless units are used throughout, it will be helpful here to work with variables carrying their proper physical dimensions.

The main point in the mechanism suggested in section 6 is that particles arriving at the inlet of the double section randomly select either of branches A or B, and particles leaving the double section through the outlet randomly originate from either of branches A or B. Furthermore, these random processes are taken to be *independent*. Their net effect has been seen to be a change in particle number of a given branch (branch A, say), of 0 (with probability 1/2) or ± 1 (with

probability 1/4 each). The total change of particles ΔN_A since the starting value therefore follows a standard random walk, except that there is a 50% chance of not moving at all. Furthermore $\Delta N_B = -\Delta N_A$ must be strictly anticorrelated due to the fact that the MC phase cannot absorb particles. Since the extra particles are swept downstream and therefore ultimately pile up to change the length of the HD region, we can therefore relate this process to the random walk of the centre of the jam, which we undertake to characterize by a diffusion constant.

Further consideration is required, however, since this effective shifting of one particle from one branch to the other displaces the domain wall *not* by the distance δ separating two neighbouring sites, but rather by

$$\tilde{\delta} = \frac{1}{\rho_{HD} - \rho_{LD}} = \sqrt{2}\,\delta. \tag{A.1}$$

Here we have used the fact that a domain wall separates an HD and an LD zone, with a density difference of $(\rho_{HD} - \rho_{LD})$, which may be evaluated using equation (3). The random walk of the jam centre X therefore involves a step size of $\tilde{\delta} = \sqrt{2}\,\delta$. Consequently, the associated diffusion constant may *not* be interpreted directly as that of the jam centre, which evolves in steps of the lattice constant δ. We must therefore consider a different time interval, say T, such that the domain walls in A and B (and hence the jam centre) displace by a multiple of the lattice constant δ (i.e. by 0 or $\pm\delta$). Since the current $J_{MC} = 1/(4\Delta t) = 1/\tilde{T}$ in the common branch supplies $n = J_{MC}\,T$ particles over the interval T, the latter is determined by matching the resulting jam displacement onto the lattice constant

$$\frac{n}{\rho_{HD} - \rho_{LD}} = \delta, \tag{A.2}$$

which therefore fixes the elementary time step as

$$T = \frac{\tilde{T}}{\sqrt{2}} = \frac{4\Delta t}{\sqrt{2}}. \tag{A.3}$$

The relevant time interval is therefore *shorter*. The average mean-square displacement of the random walk associated with the jam centre, with the time interval T separating successive steps[7], is then given as a function of time by

$$\begin{aligned}\langle \Delta X^2 \rangle &= \left(\frac{1}{4}(+\delta)^2 + \frac{1}{2}(0) + \frac{1}{4}(-\delta)^2\right)\frac{t}{T} \\ &= \frac{\delta^2}{2}\,\frac{\Delta t}{T}\,\frac{t}{\Delta t} = \frac{\delta^2}{2}\,\frac{\sqrt{2}}{4}\,\frac{t}{\Delta t}.\end{aligned} \tag{A.4}$$

Using the definition of the associated diffusion constant $\langle \Delta x^2 \rangle = 2Dt$ yields therefore

$$D_{JAM} = \frac{\sqrt{2}}{16}\,\frac{\delta^2}{\Delta t}, \tag{A.5}$$

[7] It may be worth pointing out that, somewhat subtly, adapting the time interval in this way is *different* from deducing a diffusion constant of the random walk in units of an 'effective' rescaled step size $\tilde{\delta} = \sqrt{2}\,\delta$, with a time interval of $\tilde{T}$. Such an intuitively appealing argument would not in fact be correct, since the displacement of the jam (e.g. as monitored in a simulation) evolves in steps of δ. These arise randomly, whereas operating in terms of the 'stretched' steps $\tilde{\delta}$ would introduce an (erroneous) element of persistency between successive steps. The argument of a rescaled effective step size would therefore *overestimate* the diffusion constant.

in the natural units used for the particle displacements (step size δ and time step Δt), as announced in the main text.

Appendix B. Domain wall localization via mesoscopic time averages

We detail here the algorithm we have used for locating the domain wall (DW) positions on the transport plateau (cf figure 2), and in particular for the diagrams shown in figure 7. It relies on exploiting a 'mesoscopic' timescale, intermediate between the microscopic fluctuations in the occupation number of a given site and a macroscopic regime in which mean-field theory describes the average density profiles. For times of the order of individual simulation cycles, the occupation number of a given site may fluctuate, and any such fluctuation may create an additional micro domain wall (μDW, defined as an interface between an empty and an occupied site), or destroy such a μDW. In order to extract positions of a macroscopic DW we therefore have to consider a timescale τ which is much larger than the fluctuation of individual site occupation, but much smaller than DW migration (equivalent to jam diffusion described above). In order to determine this timescale we sample instantaneous site occupation over a time τ in order to establish a partially time-averaged density on a given site as

$$\rho_\tau(x,t) = \frac{1}{\tau}\sum_{i=1}^{\tau}\rho(x,t+i). \tag{B.1}$$

The number of μDWs in branch A or B, at a given time t, is then determined by following these densities along the branch and counting how many times we cross the value 0.5 (on the increase or on the decrease). In the stationary state

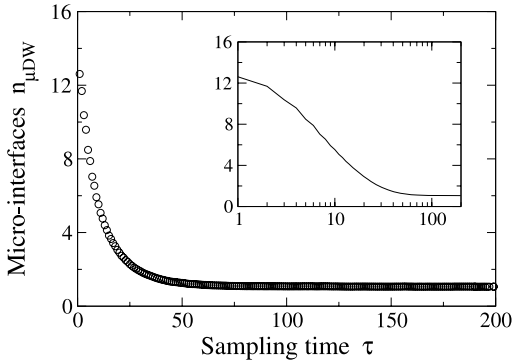

Figure B.1. The number of micro domain walls (μDWs) in the split branches of current-saturated HEX-TASEP, as a function of the 'mesoscopic' averaging time τ. A μDW is defined as a jump in pre-averaged particle density crossing the value 1/2 (see the main text). Data have been obtained for a HEX-TASEP simulation of $3L + 2$ sites ($L = 100$), at an overall density of $\rho = 0.5$. For each 'mesoscopic' sampling time τ, the simulation was run for 10^5 sampling times. For large enough sampling times, $\tau \approx 100$ or larger, there is only one μDW per branch, which must correspond to the macroscopic domain wall we wish to localize, and we conclude that a sampling time of $\tau = 100$ is an appropriate choice. The inset is a logarithmic plot of the same data, highlighting the asymptotic approach to the sampling time required such that only the macroscopic domain wall is detected.

the time evolution of this pre-averaged quantity converges to a long-time value. The resulting number of μDWs in the stationary state is shown in figure B.1 for HEX-TASEP of one unit cell and with periodic boundary conditions. The graph confirms what is intuitively expected: the number of μDWs decreases with the sample time τ, until only one interface is left, which corresponds to the macroscopic DW. In order to unambiguously locate the macroscopic DW, sampling is required over a time of $\tau \approx 100$, which is the value stated in the main text. This time interval is furthermore sufficiently short that the DW has not diffused over a large distance (cf figure 6), and the DW position so localized may therefore indeed be used to characterize their dynamics, as in figure 7. In practice we found this algorithm to be simple to use and robust, avoiding the subtleties associated with so-called second-class particles [21].

References

[1] Wei Q-H, Bechinger C and Leiderer P 2000 Single-file diffusion of colloids in one-dimensional channels *Science* **287** 625–7

[2] Lutz C, Kollmann M, Leiderer P and Bechinger C 2004 Diffusion of colloids in one-dimensional light channels *J. Phys.: Condens. Matter* **16** S4075–83

[3] Roux A, Cappello G, Cartaud J, Prost J, Goud B and Bassereau P 2002 A minimal system allowing tubulation with molecular motors pulling a giant liposome *Proc. Natl Acad. Sci.* **99** 5394–9

[4] Koster G, VanDuijn M, Hofs B and Dogterom M 2003 Membrane tube formation from giant vesicles by dynamic association of motor proteins *Proc. Natl Acad. Sci.* **100** 15583–8

[5] Leduc C, Campas O, Zeldovich K B, Roux A, Jolimaitre P, Bourel-Bonnet L, Goud B, Joanny J-F, Bassereau P and Prost J 2004 Cooperative extraction of membrane nanotubes by molecular motors *Proc. Natl Acad. Sci.* **101** 17096–101

[6] Kukla V, Kornatowski J, Demuth D, Girnus I, Pfeifer H, Rees L V C, Schunk S, Unger K K and Körger J 1996 NMR studies of single-file diffusion in unidimensional channel zeolites *Science* **272** 702–4

[7] MacDonald C T, Gibbs J H and Pipkin A C 1968 Kinetics of biopolymerization on nucleic acid templates *Biopolymers* **6** 1–5

[8] Derrida B, Domany E and Mukamel D 1992 An exact solution of a one-dimensional asymmetric exclusion model with open boundaries *J. Stat. Phys.* **69** 667–87

[9] Schütz G and Domany E 1993 Phase transitions in an exactly soluble one-dimensional exclusion process *J. Stat. Phys.* **72** 277

[10] Pierobon P, Parmeggiani A, von Oppen F and Frey E 2005 Dynamic correlation functions and Boltzmann–Langevin approach for driven one-dimensional lattice gas *Phys. Rev.* E **72** 036123

[11] Schütz G M 2000 *Exactly Solvable Models for Many-Body Systems Far from Equilibrium* (London: Academic) and references therein

[12] Privman V (ed) 1997 *Nonequilibrium Statistical Mechanics in One Dimension* (Cambridge: Cambridge University Press)

[13] Pollard T D 2003 The cytoskeleton, cellular motility and the reductionist agenda *Nature* **422** 741–5

[14] Meloy J R, Neethling S J and Cilliers J J 2007 Geometric dispersion of unattached particles in foams *Colloids Surf.* A **309** 246

[15] Schadschneider A 2000 Statistical physics of traffic flow *Physica* A **285** 101

[16] Pronina E and Kolomeisky A B 2005 Theoretical investigation of totally asymmetric exclusion processes on lattices with junctions *J. Stat. Mech.* **07** P07010

[17] Brankov J, Pesheva N and Bunzarova N 2004 Totally asymmetric exclusion process on chains with a double-chain section in the middle: computer simulations and a simple theory *Phys. Rev.* E **69** 066128

[18] Helbing D 2001 Traffic and related self-driven many-particle systems *Rev. Mod. Phys.* **73** 1067–141

[19] Kolomeisky A B, Schütz G M, Kolomeisky E B and Straley J P 1998 Phase diagram of one-dimensional driven lattice gases with open boundaries *J. Phys. A: Math. Gen.* **31** 6911–9

[20] Santen L and Appert C 2002 The asymmetric exclusion process revisited: fluctuations and dynamics in the domain wall picture *J. Stat. Phys.* **106** 187–99

[21] Boldrighini C, Cosimi G, Frigio S and Grasso Nuñes M 1989 Computer simulation of shock waves in the completely asymmetric simple exclusion process *J. Stat. Phys.* **55** 611–23